Effect of the soil water dynamics on nitrous oxide emissions

E. Rabot, Catherine Hénault, Isabelle Cousin

Effect of the soil water dynamics on nitrous oxide emissions

E. Rabot, C. Hénault, I. Cousin *

INRA, UR0272, UR Science du Sol, F-45075 Orléans, France

Microbial N_2O production may occur via denitrification, a reaction which is influenced by the soil's water content. This study aimed to test the effect of soil water dynamics on N_2O production and transport. The treatments consisted of two levels of soil bulk density (BD), negative pressure head applied on the soil cylinder (H), and saturated hydraulic conductivity of the ceramic plate placed at the bottom of the soil sample (K). We controlled the water status of repacked soil samples during two wetting-drying cycles, by using a multistep outflow system. The matric potential, outflow, N_2O, and CO_2 fluxes were recorded over time. A brief N_2O peak occurred at the beginning of soil drying: N_2O produced and entrapped in the soil during the wetting phase was released during soil drying with the increase in soil gas diffusion. Similar peaks dynamics were observed for CO_2, implying that a physical process was involved. A relationship was observed to occur with maximum N_2O fluxes increasing exponentially with cumulative drainage. Indeed, during drying, high N_2O fluxes were measured when the air-entry potential was reached, i.e., when gas pathways were available for fast N_2O transport in the gas phase. Then, maximum and cumulative N_2O fluxes were highest for low BD and fast water flow during drying. Samples with the highest BD had smaller pore sizes, leading to low outflows at a given negative pressure head, and giving more time for further reduction of N_2O to N_2. We ranked the importance of the parameters controlling cumulative N_2O fluxes: H > BD > K.

1. Introduction

Soils are a major source of nitrous oxide (N_2O), a potent greenhouse gas, as they account for two thirds of the anthropogenic N_2O sources, in particular through agricultural practices and the use of fertilizers (Ciais et al., 2013). Because the N_2O concentration in the atmosphere is still increasing (Khalil et al., 2002), reliable data and a better knowledge of N_2O emission processes are needed.

Under oxygen (O_2) limited conditions, N_2O formation is dominated by denitrification (Bateman and Baggs, 2005). Among others, this reaction is influenced by the soil water content, because of its role as a barrier to O_2 transport (Kroeckel and Stolp, 1986). Indeed, anaerobic conditions are required for denitrifying bacteria to reduce nitrate and form N_2O. At very high soil water contents, N_2O reduction to dinitrogen (N_2) occurs (Ruser et al., 2006). Thus, in the literature, attention has been paid to the role of soil water content and N_2O emissions. For instance, N_2O peaks have frequently been observed from the rewetting of dry soils (Groffman and Tiedje, 1988; Harrison-Kirk et al., 2013; Sexstone et al., 1985). Their magnitude have partly been explained by the degree of anaerobiosis of the soil, estimated using water-filled pore space (WFPS) (Beare et al., 2009; Harrison-Kirk et al., 2013; Linn and Doran, 1984), soil matric potential (Balaine et al., 2013; Castellano et al., 2010; Kroeckel and Stolp, 1986), or redox potential (Ciarlo et al., 2007). In addition, the processes involved in the emissions of N_2O from soils, subjected to wetting and drying cycles, depend on the magnitude and temporal dynamics of the wetting-drying cycles. Indeed, Guo et al. (2014) observed that N_2O emissions were higher when the drying phase was severe and the degree of wetting was high. Muhr et al. (2008) and Rabot et al. (2014) also reported that the N_2O emissions intensity decline after several wetting and drying cycles.

Delays between the microbial N_2O production and the moment when N_2O is measured at the soil surface have been demonstrated (Clough et al., 1998; Rabot et al., 2014; Weier et al., 1993; Wollersheim et al., 1987). Xing et al. (2011) observed their highest N_2O fluxes between 1 and 10 h after the peak of WFPS. Delays in N_2O emission are partly linked to entrapment in the gas phase, due to the presence of water occupying soil pores and the associated N_2O dissolution in the water phase (Clough et al., 2005). McNicol and Silver (2014) separated the effects of the water content and anoxia level on N_2O emissions, by flooding a soil sample or creating an anaerobic headspace. They showed that N_2O production was sensitive to the redox effects of O_2 depletion and that flooding can have additional effects on gas entrapment and transport, and availability of the dissolved solutes. Because of N_2O entrapment in the gas and liquid phases during the water saturation of soils, Rabot et al. (2014) recorded high N_2O fluxes during soil drying. They showed a positive correlation between the outflow and the intensity of N_2O fluxes. The study of Rabot et al. (2014)

* Corresponding author.
E-mail address: isabelle.cousin@orleans.inra.fr (I. Cousin).

demonstrated that the physical role of water was the principle cause of high N_2O emissions, when compared with direct and immediate N_2O production, because entrapped N_2O was released during soil drying. This was also demonstrated by Balaine et al. (2013) who showed that maximum N_2O fluxes occurred during drainage when the soil's air-entry potential was reached, allowing O_2 to enter the soil, inhibiting denitrification, and allowing N_2O entrapped in the soil to diffuse out.

Although substantial efforts have been made to study the relationship between the WFPS, or the intensity of soil wetting and drying, on N_2O emissions, these studies have mainly focused on the N_2O production process. Because N_2O emissions are influenced by both aerobic conditions and water flow, this study aimed at understanding the effect of the soil water dynamics on both N_2O production and transport, by performing wetting-drying cycle experiments under controlled conditions. To complete the observations of the Rabot et al. (2014) study, three variables known for affecting the water flow were assessed in this experiment: we used repacked soil samples to control the soil structure and therefore, the hydraulic properties of the soil samples, and we designed the experiment to control the amount and speed of water drainage.

2. Material and methods

2.1. Soil samples

Soil material was collected in February 2013, from the surface horizon (0–10 cm) of a Glossic Retisol (IUSS Working Group WRB, 2014). The study site was located near Chartres, in the northwest of France (48.376° N, 1.196° E), at the same location as the study of Rabot et al. (2014). This study site was chosen because of the high N_2O emissions previously recorded in the field (Gu et al., 2011). At sampling time, the field was cultivated with rape (*Brassica napus* L.). Samples had a silt loam texture composed of 13.7% clay (<2 μm), 82.0% silt (2–50 μm), and 4.3% sand (50–2000 μm) (Rabot et al., 2014). The soil pH (water) was 6.5, the soil organic carbon was 9.0 g kg^{-1}, the total nitrogen content was 1.09 g kg^{-1}, and the nitrate content was 55.9 mg NO_3^-–N kg^{-1}.

The bulk soil was first dried at 25 °C, sieved to <5 mm, and mixed. The water content of the soil dried at 25 °C was determined by oven drying an aliquot at 105 °C. This value was used to wet the soil dried at 25 °C to 20% gravimetric water content before packing to specific bulk densities (see Section 2.2.2) in 15-cm inner diameter by 7-cm high cylinders.

2.2. Water control and monitoring

2.2.1. Description of the water control system

In this experiment, the water status of each soil core was controlled with the multistep outflow system described in Rabot et al. (2015). This system allowed several wetting-drying cycles to be applied without moving the soil core, while controlling the wetting and drying intensities. In this system, the soil core was connected to a water tank to control its wetting from the bottom, and connected to a vacuum pump to control its drainage from the bottom. Hydraulic continuity at the bottom of the soil core was ensured with a 1-cm high porous ceramic plate (Soilmoisture Equipment Corp.) previously saturated with water. The outflow was collected in a sampling bottle and its weight was monitored with a balance (0.1 g precision). The outflow was used to estimate the WFPS of the soil sample. The water potential was monitored with three microtensiometers (porous ceramic cup, 20-mm length, 2.2-mm diam., 150-kPa air-entry value) inserted at three depths from the soil surface (0.5, 1, and 2 cm). Data were recorded every 10 min with a datalogger (CR1000, Campbell Scientific). The temperature in the room ranged between 20 and 21 °C.

2.2.2. Experimental design

The soil core was first saturated for four days with the multistep outflow system, by raising the water level to the soil surface in one step, until a water layer (≈2 mm) was visible at the soil surface. Then a negative pressure was applied in one step at the bottom of the soil core with the vacuum pump, and maintained for three days. This wetting and drying cycle was applied two times (hereafter referred to as C1 and C2 cycles), to observe if there was a consistency in the N_2O emissions between the first and second cycle.

To evaluate the effect of the water dynamics on N_2O emissions, three variables known for affecting directly or indirectly the water flow were crossed, in a full factorial design: the soil bulk density (BD), the negative pressure applied on the soil sample (H), and the saturated hydraulic conductivity of the ceramic plate placed at the bottom of the soil sample (K). Each of the three factors had two levels, leading to eight different treatments. Each treatment was replicated three times, giving a total of 24 soil samples. These factors and their respective levels are summarized in Table 1.

- Repacked soil samples were used in this study to control the soil structure. The soil BD was varied between the two levels, by packing a known soil mass inside the 15-cm diameter by 7-cm height cylinders. Their values were chosen to be typical of the agricultural areas of the study site. BD directly affects the pore volume, pore diameters, and tortuosity of the pore network.
- The H value was controlled with the vacuum pump. Rabot et al. (2014) demonstrated that N_2O peaks can be created during the drying phase for matric potentials of about −50 and −100 hPa. We chose thus to apply a pressure of −100 hPa and −300 hPa, to study much dryer conditions.
- Finally, at a given H, the speed of the water drainage was also varied depending on the saturated hydraulic conductivity K of the ceramic plate placed at the bottom of the soil sample. The ceramic plates used in the experiment had a saturated hydraulic conductivity of 8.6×10^{-8} m s^{-1} for the high flow (HF) level, and 7.6×10^{-9} m s^{-1} for the standard flow (SF) level, both with an air-entry potential <−1000 hPa. They mimic a soil horizon of low hydraulic conductivity, such as the clay illuviation horizon located below the sampled horizon of the studied Glossic Retisol.

Given that we worked in the near-saturation range, which is a level of water content that is typically involved in the denitrification process (Mathieu et al., 2006), we used nitrate as the substrate for N_2O production. The wetting fluid was a KNO_3 solution with a nitrate concentration (575 mg N L^{-1}) assumed to be large enough so that it was not a limiting factor for N_2O production by denitrification (Hénault and Germon, 2000), therefore allowing isolation of soil moisture effects. The nitrate solution was prepared with deaired water to prevent air bubble formation during the experiment.

2.3. Gas measurements

The multistep outflow system for water control was coupled with a N_2O analyzer measuring N_2O concentrations using gas filter correlation in the infrared region (N_2O Analyzer Model 46i, Thermo Scientific). A 4-L-volume closed-chamber was fixed over the soil during N_2O

Table 1
Factors used in the study and their levels.

Factors	Levels	
Soil bulk density (BD)	1.35 g cm^{-3}	1.45 g cm^{-3}
Pressure head (H)	−100 hPa	−300 hPa
Hydraulic conductivity of the ceramic plate (K)	High flow (HF) 8.6×10^{-8} m s^{-1}	Standard flow (SF) 7.6×10^{-9} m s^{-1}

measurements. It was removed before the start of each measurement to restore the atmosphere to an ambient N_2O concentration. Accumulation of gases was measured for 20-min periods, three to eight times a day. The N_2O concentration value was recorded every minute. Given the linear increase in the N_2O concentration, N_2O fluxes were calculated linearly from the observed change in concentration during 10-min periods. Moreover, at the end of the day, gases inside the chamber were sampled in evacuated vials, and the carbon dioxide (CO_2) concentration was determined by gas chromatography (μGC Gas Analyzer T-3000, SRA Instruments), in order to compare its dynamics with N_2O. For a single CO_2 flux measurement, the atmosphere of the closed-chamber was sampled three times during a 20-min period. CO_2 flux was then calculated linearly. N_2O and CO_2 fluxes were recorded, i) on the first and the last days of the wetting phase, and ii) every day during the drying phase. The soil nitrate content was determined at the end of the experiment as an indicator of total denitrification. Nitrate content was measured by colorimetric analysis (Hach Lange, DR 2800), after extraction from an 8-g soil sample using 0.5 mol L^{-1} K_2SO_4.

2.4. Hydraulic characterization and modeling of the water dynamics

In order to characterize the water retention of the samples and to model the water dynamics as function of time, we measured two basic soil hydraulic characteristics, the saturated hydraulic conductivity and the water retention curve.

The saturated hydraulic conductivity (K_s) describes the ability of soils to conduct water. It was measured on two soil samples packed at BD = 1.35 and 1.45 g cm^{-3}, with the falling head method, by using the KSAT commercial device (UMS).

The soil water retention curve gives the relation between soil water content and matric potential. It was determined on additional soil samples at BD = 1.35 and 1.45 g cm^{-3} with the evaporation method (Tamari et al., 1993; Wind, 1968). In this method, after wetting to saturation, the soil sample was subjected to evaporation under laboratory conditions. The evolution of the soil water content with time was monitored by continuously weighing the soil sample. Five microtensiometers were inserted into the soil cylinder to measure the matric potential. By using the ESPAS algorithm (Ruy et al., 2004), the soil water retention curve was then adjusted according to the van Genuchten (1980) model (Eq. 1).

$$\frac{\theta\text{-}\theta_r}{\theta_s\text{-}\theta_r} = \frac{1}{\left[1+(\alpha h)^n\right]^m} \quad (1)$$

where h is the matric potential (m), θ is the volumetric water content ($cm^3\ cm^{-3}$), θ_s is the saturated water content ($cm^3\ cm^{-3}$), θ_r is the residual water content ($cm^3\ cm^{-3}$), α (m^{-1}), n and m are curve fitting parameters, with $m = 1 - 1/n$.

The pore size distribution of the samples was derived from this water retention curve. We converted first the measured water retention curve $\theta = f(h)$ into an equivalent $\theta = f(d)$ curve, with d the maximum water-filled pore diameter (m): at a given h, d was estimated from the Jurin's law (Eq. 2). The derivative of this curve gives the pore size distribution.

$$d = \frac{4\sigma\cos(\gamma)}{\rho g|h|} \quad (2)$$

where σ is the surface tension of water (N m^{-1}), γ is the contact angle of water, ρ is the density of water (kg m^{-3}), and g is the gravitational acceleration (m s^{-2}).

We simulated the evolution of the water flux, i.e., the volume of water per area and per unit of time, during drying. The Mualem (1976) and van Genuchten (1980) equations used in the model were parameterized with the measured water retention curve, the soil saturated hydraulic conductivity, and data from the ceramic plate manufacturer. Simulations were performed by solving the Richards' equation with the Hydrus-1D software (Simunek et al., 2008), in its direct configuration. We simulated a 7-cm high soil sample located above a 1-cm high porous ceramic plate, with 161 nodes. No-flux boundary condition was imposed at the upper boundary. At the lower boundary, the imposed pressure head either varied from saturation to −100 hPa or from saturation to −300 hPa. The initial pressure head corresponded to the saturation of the soil sample.

2.5. Data analyses

To analyze the experimental data, the cumulative N_2O and CO_2 fluxes were calculated by linearly interpolating the flux values that were recorded with time, then integrating the area under the curve. These calculations were realized with the MESS package (Ekstrom, 2014) built on R (R Core Team, 2015). The effect of the three BD, H and K variables, and of the hydric period were assessed by using the nonparametric test of Mann-Whitney at the 5% level. Correlations were assessed by the calculation of Spearman correlation coefficients. A three-way analysis of variance (ANOVA) was used to assess the relative influence of BD, H, and K on the cumulative N_2O emissions, by calculating the effect size (Eta squared) of the three controlled parameters and of their interactions. Because cumulative N_2O fluxes were not normally distributed, they were first log transformed. In the following, both the means and their associated standard errors are reported.

3. Results

3.1. Soil water dynamics

Hydraulic parameters, describing the water retention curve according to the van Genuchten (1980) model, were quite similar for the two levels of BD (Table 2). The difference in BD led to differences in the saturated water content θ_s and air-entry potential. The air-entry potential, i.e., the negative pressure at which the sample starts to drain, was calculated as the inverse of the α parameter (Table 2). The air-entry potential was −68 hPa and −118 hPa for the BD = 1.35 and BD = 1.45 g cm^{-3} samples, respectively. So, the air-entry potential was reached at the end of the drying phase for the two H levels (i.e., −100 and −300 hPa) for BD = 1.35 g cm^{-3} samples, but only for the −300 hPa level for BD = 1.45 g cm^{-3} samples. As expected, K_s was slightly higher for BD = 1.35 than for BD = 1.45 g cm^{-3} samples (Table 2).

The pore size distributions derived from the water retention curves are shown in Fig. 1. The modal pore diameter was 12 and 8 μm for the BD = 1.35 and BD = 1.45 g cm^{-3} samples, respectively. The BD = 1.35 g cm^{-3} samples had a higher volume of pores >10 μm in diameter than the BD = 1.45 g cm^{-3} samples. For pores <10 μm in diameter, corresponding to the textural porosity of the aggregates, the difference between the two levels of BD was less pronounced.

An example of the measured matric potential dynamics is given in Fig. 2 for a sample of BD = 1.45 g cm^{-3}, H = −300 hPa, and K = HF. As soon as the vacuum pump was activated, the soil matric potential first decreased abruptly, and then decreased more slowly to finally reach a plateau. In this example, the hydraulic equilibrium was not reached after three days of soil drying for C1, as the minimum recorded matric potential was −260 hPa, but it was reached at the end of C2. During the C2 rewetting, the increase of the soil matric potential to 0 hPa took 2 h in this example.

The measured WFPS at the end of each wetting and drying phases are given in Table 3. The WFPS ranged between 98.3 and 57.4% during C1, and between 98.3 and 61.2% during C2 for the BD = 1.35 g cm^{-3} samples. It ranged between 101.8 and 71.2% during C1, and between 101.2 and 69.1% during C2 for the BD = 1.45 g cm^{-3} samples. Values higher than 100% were linked to a surface water layer during the wetting phase. WFPS was higher for BD = 1.45 than for BD = 1.35 g cm^{-3} samples for each wetting and drying phases ($p < 0.05$).

Table 2
Estimated hydraulic parameters of the samples of bulk density BD = 1.35 and 1.45 g cm^{-3}.

Bulk density	θ_s	θ_r	α	n	m	K_s
(g cm^{-3})	(cm cm^{-3})		(m^{-1})			(m s^{-1})
1.35	0.49	1.77×10^{-5}	1.433	1.262	0.208	2.57×10^{-7}
1.45	0.46	7.96×10^{-5}	0.833	1.282	0.220	1.79×10^{-7}

Considering the effect of the two wetting-drying cycles, no significant difference in the WFPS value was found between the C1 and C2 wetting phases, or between the C1 and C2 drying phases ($p > 0.05$). Thus, the first and second cycles were similar from a hydric point of view. However, higher WFPS were generally observed at C2 than at C1 during the drying phase for BD = 1.35 g cm^{-3} samples (non-significant, $p > 0.05$). Considering the effect of the H and K variables during the drying phase, an effect of H was found, where the lowest WFPS were found for H = −300 hPa, for BD = 1.35 and BD = 1.45 g cm^{-3} samples ($p < 0.05$). During the drying phase, an effect of K was also found for BD = 1.35 g cm^{-3} samples ($p < 0.05$), because the SF level tended to produce samples with a slightly higher WFPS.

3.2. Nitrous oxide fluxes

An example of the N_2O flux dynamics is also presented in Fig. 2 for the sample of BD = 1.45 g cm^{-3}, H = −300 hPa, and K = HF. Fluxes remained low during the C1 and C2 wetting phases. However, a small N_2O peak could be seen at the very beginning of the C1 wetting phase, lasting approximately 8 h. This peak has been observed in each sample of our data set. Higher N_2O peaks were then observed at the beginning of the C1 and C2 drying phases (in the example of Fig. 2, the maximum was observed after 4.1 h for C1 and 1.3 h for C2). The peak was higher for C1 than for C2 (in the example of Fig. 2, 433.7 mg N m^{-2} d^{-1} for C1 and 336.1 mg N m^{-2} d^{-1} for C2). After these two peaks, fluxes returned to a baseline after 24 h of soil drying, when the matric potential became closer to equilibrium. The dynamics of this example were representative of the dynamics of all the studied soil samples.

Maximum measured N_2O fluxes were higher for the drying phases than for the wetting phases ($p < 0.0001$), except for the BD = 1.45 g cm^{-3}, H = −100 hPa, K = SF treatment (Fig. 3). Whatever the treatment, fluxes were higher for the C1 wetting phase than for the C2 wetting phase ($p < 0.0001$). On the contrary, no significant difference was found between the C1 drying phase and the C2 drying phase ($p > 0.05$). An effect of K was found for BD = 1.35 g cm^{-3} samples at the C1 drying phase ($p < 0.05$, Fig. 3), whereas an effect of H was found for BD = 1.45 g cm^{-3} samples at the C1 drying, C2 wetting, and C2 drying phases ($p < 0.05$, Fig. 3). The maximum N_2O flux during the peak of the drying phase could be described by an exponential relationship with the measured cumulative outflow (Fig. 4). Fig. 4 also shows that the cumulative outflow was generally lower for the BD = 1.45 than for the BD = 1.35 g cm^{-3} samples.

Cumulative N_2O fluxes ranged between 278 and 577 mg N m^{-2} d^{-1} for BD = 1.35 g cm^{-3} samples, and between 130 and 561 mg N m^{-2} d^{-1} for BD = 1.45 g cm^{-3} samples (Fig. 5). Cumulative N_2O fluxes were generally higher for BD = 1.35 than for BD = 1.45 g cm^{-3} samples, except for the H = −300 hPa and K = SF treatment (Fig. 5). The relative contribution of the drying phase in the cumulative N_2O fluxes was 51 ± 7% for BD = 1.35 g cm^{-3} samples, and 40 ± 7% for BD = 1.45 g cm^{-3} samples. Like for the maximum N_2O fluxes, an effect of K was found for BD = 1.35 g cm^{-3} samples ($p < 0.05$, Fig. 5), where the highest saturated hydraulic conductivity of the ceramic plate led to the highest N_2O fluxes. For the BD = 1.45 g cm^{-3} samples, an effect of H was found ($p < 0.05$, Fig. 5), where the lowest pressure applied at the bottom of the soil core led to the highest N_2O fluxes. By comparing the two wetting-drying cycles, we found that cumulative N_2O fluxes were higher for C1 than for C2 during the wetting phase ($p < 0.0001$) whatever the treatment, and was higher for C1 than for C2 during the drying phase for 2/3 of the soil samples. The relative contribution of the C1 cycle compared with C2 was 69 ± 4%. The cumulative N_2O flux at the end of the two wetting-drying cycles was correlated with the total outflow ($R = 0.68$, $p < 0.001$, removing one outlier of the BD = 1.45 g cm^{-3}, H = −100 hPa, K = SF treatment). The ANOVA performed for the whole data set on the log transformed cumulative N_2O emissions and the controlled H, BD, and K gave $R^2 = 0.78$. The proportion of variance explained by the controlled factors was given by the Eta squared scores, and was 37% for H, 12% for BD, and 5% for K (Table 4). The interaction between BD and H was significant, accounting for another 13%, and the interaction between BD and K for 6% (Table 4).

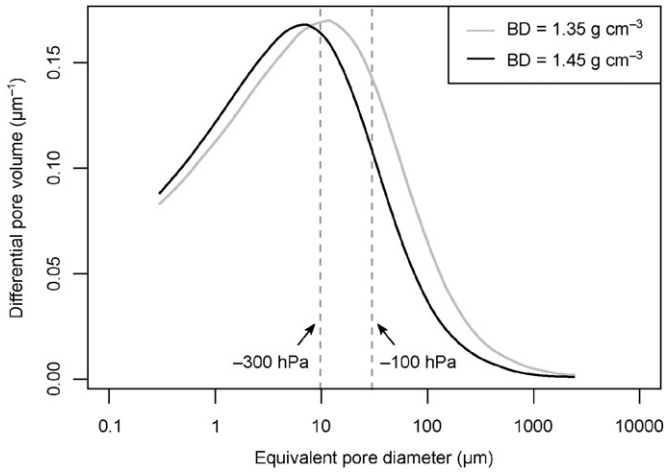

Fig. 1. Pore size distribution, derived from the water retention curve, of soil samples of bulk density BD = 1.35 and 1.45 g cm^{-3}.

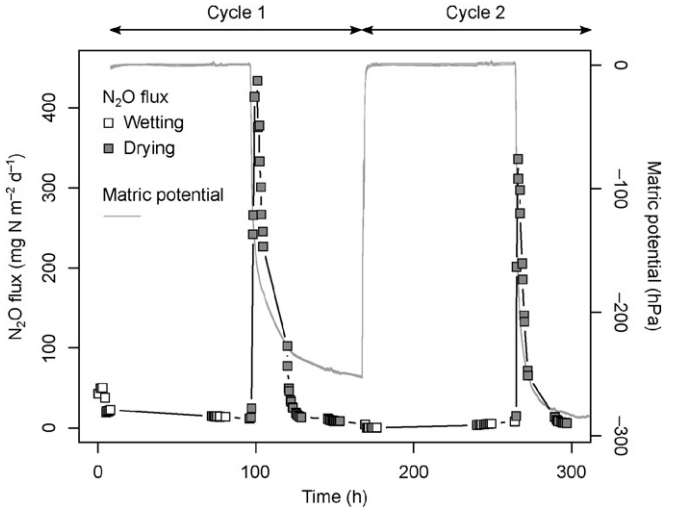

Fig. 2. Evolution with time of the nitrous oxide fluxes and matric potential of a sample of bulk density BD = 1.45 g cm^{-3}, pressure head applied H = −300 hPa, and a high flow porous plate, during two wetting-drying cycles. For the sake of readability, the measurement points are linearly interpolated.

Table 3
Evolution of the water-filled pore space and soil nitrate concentration (mean ± standard error) at the end of the first (C1) and the second (C2) wetting-drying phases (BD: bulk density, H: pressure head applied, K: saturated hydraulic conductivity of the porous plate, HF: high flow, SF: standard flow).

Treatment			Water-filled pore space (%)				NO_3^-–N
BD	H	K	C1 wetting	C1 drying	C2 wetting	C2 drying	C2 drying
(g cm^{-3})	(hPa)						(mg N kg^{-1})
1.35	−100	HF	98.3 ± 0.5	72.4 ± 0.2	98.3 ± 0.5	77.9 ± 1.0	145.9 ± 9.9
1.35	−100	SF	97.7 ± 0.4	75.7 ± 7.7	97.6 ± 0.3	87.1 ± 1.1	136.7 ± 16.3
1.35	−300	HF	95.4 ± 1.7	57.4 ± 2.7	95.3 ± 1.7	61.2 ± 3.4	111.6 ± 13.6
1.35	−300	SF	94.5 ± 1.6	64.1 ± 4.7	94.5 ± 1.6	72.4 ± 4.5	97.6 ± 9.3
1.45	−100	HF	101.2 ± 0.8	91.1 ± 1.6	101.2 ± 0.8	95.4 ± 0.7	78.6 ± 10.4
1.45	−100	SF	98.4 ± 0.4	88.0 ± 1.0	98.3 ± 0.4	89.5 ± 2.0	74.2 ± 5.7
1.45	−300	HF	98.7 ± 0.8	71.2 ± 2.9	98.7 ± 0.8	69.1 ± 0.5	65.9 ± 3.2
1.45	−300	SF	101.8 ± 2.5	85.5 ± 6.9	100.7 ± 3.6	85.0 ± 6.9	78.8 ± 9.6

3.3. Auxiliary variables

Trends in the CO_2 flux dynamics were similar to those of the N_2O fluxes, except for the H = −100 hPa, K = SF samples (Fig. 6). An effect of K was found at the C1 drying phase for the BD = 1.35 g cm^{-3} samples ($p < 0.05$, Fig. 6), like for N_2O. An effect of H was found during the drying phase both at C1 and C2 for the BD = 1.45 g cm^{-3} samples ($p < 0.05$, Fig. 6), like for N_2O.

The soil nitrate content at the end of the experiment was significantly higher for the BD = 1.35 than for the BD = 1.45 g cm^{-3} samples ($p < 0.0001$): it ranged from 97.6 to 145.9 mg N kg^{-1} for the BD = 1.35 g cm^{-3} samples, and from 65.9 to 78.6 mg N kg^{-1} for the BD = 1.45 g cm^{-3} samples (Table 3). A significant effect of H was found on the soil nitrate content for the BD = 1.35 g cm^{-3} samples ($p < 0.05$; Table 3), but not for the BD = 1.45 g cm^{-3} samples.

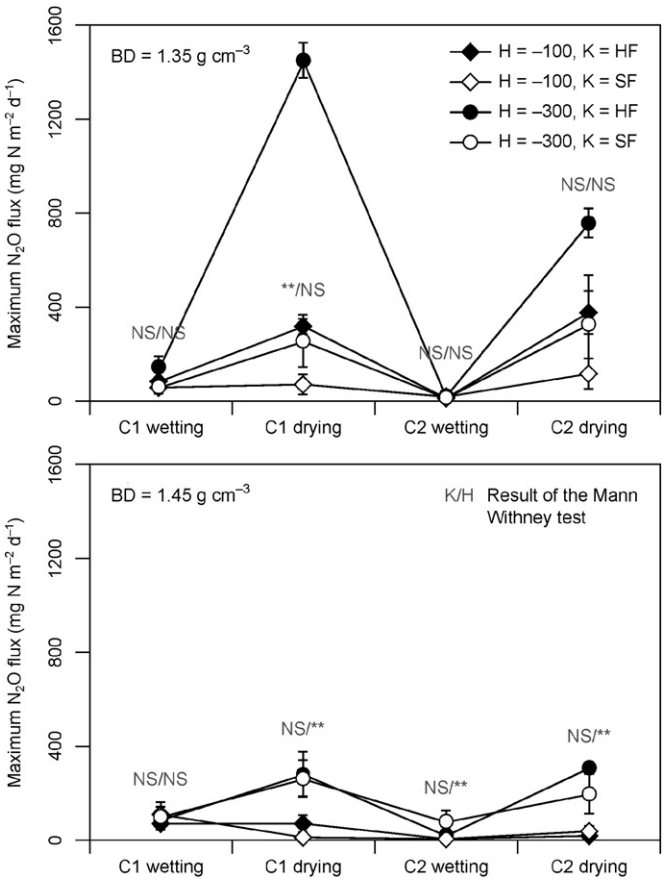

Fig. 3. Maximum nitrous oxide fluxes recorded during the four successive hydric steps (C1: first wetting-drying cycle, C2: second wetting-drying cycle) for soil samples of bulk density BD = 1.35 and 1.45 g cm^{-3} (H: pressure head applied, in hPa, K: saturated hydraulic conductivity of the porous plate, HF: high flow, SF: standard flow). Error bars represent standard error of the mean ($n = 3$).

4. Discussion

4.1. Role of the soil water dynamics

Although N_2O is known to be produced in soil samples with high WFPS (e.g., Beare et al., 2009; Grundmann and Rolston, 1987), our experiment showed N_2O fluxes which were generally higher during the drying phase than during the wetting phase. This trend was also seen with CO_2 emissions, and may be related to the lower gas diffusion into wet soils (Buckingham, 1904; Campbell, 1974). The fact that similar trends were observed for N_2O and CO_2, despite different optimal moisture conditions for their formation, highlights the role of physical processes linked to gas transport. Rabot et al. (2014) and Letey et al. (1980) showed that N_2O is likely to be entrapped in the soil during the wetting phase and to be released later during the soil drying as gas diffusion occurs. Similar behavior may have occurred here, so the intensity and speed of N_2O emissions will be discussed from this point of view.

In the cumulative and maximum N_2O flux data, the most intense N_2O emissions were generally recorded during the drying phase caused by a low pressure head applied at the bottom of the soil core (H) and a high hydraulic conductivity of the ceramic plate (K). However, the effect of K was dominating for BD = 1.35 g cm^{-3}, whereas the effect of H was dominating for BD = 1.45 g cm^{-3}. Cumulative N_2O fluxes were generally higher for BD = 1.35 than for BD = 1.45 g cm^{-3} samples. These trends can be explained by the dynamics of water.

Simulated profiles of water fluxes just after the beginning of the soil drying of a BD = 1.35 g cm^{-3} sample are presented in Fig. 7, for a period of 200 min (3.3 h), corresponding to the phase of increase in the recorded N_2O fluxes. The speed of the water drainage as function of time can thus be observed. For higher K, the water flux was higher at the very beginning of the soil drainage, and then decreased non-linearly with time (Fig. 7c and d). The rapid N_2O transport by gas diffusion and N_2O release from the water phase would have been favored by this water movement. The same observation can be done for lower H (Fig. 7b and d). An additional effect of the H value is related to the size of the water-filled pores. According to the Jurin's law (Eq. 2), the size of the water-filled pores is smaller for lower H values. The water-filled pore size is an important factor affecting N_2O emissions (Castellano et al., 2010), because small pores are expected to be the place of microbial N_2O production and consumption (Heincke and Kaupenjohann, 1999). When these small pores drain, entrapped N_2O can be released, and the environment becomes oxic. As shown in the experiment, the K parameter also had an effect on the WFPS value at the end of the drying phase for the BD = 1.35 g cm^{-3} samples (Table 3), and thus on the water-filled pore size. To summarize, both K and H had an effect on the speed of the water drainage, with implications for the N_2O release from the water phase and emission by gas diffusion, and an additional effect on the WFPS

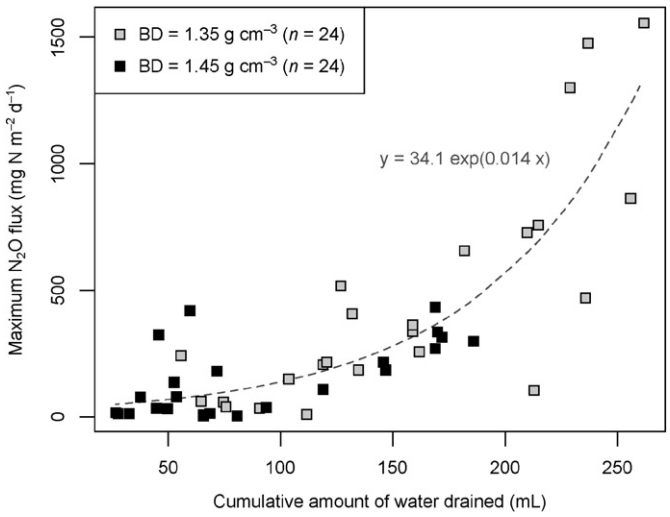

Fig. 4. Relationship between the maximum nitrous oxide flux, measured during the nitrous oxide peak of the first and the second drying phases, and the measured cumulative outflow (BD: bulk density).

value at the end of the drying phase, with implications on the N_2O production/consumption processes.

4.2. The specific case of bulk density

The effect of BD on the morphology of the pore network and water flow can also influence the intensity and speed of N_2O emissions. For higher BD, the modal pore diameter was smaller (Fig. 1), the pore volume, the air-entry potential were lower (Table 2), and the amount of pore connections to the atmosphere may be lower. These physical effects of a high value of BD do not favor the release of the entrapped N_2O.

However, considering the N_2O production, the finer pores need relatively lower pressure heads to drain (Eq. 2), which favors the water retention and establishment of anoxic conditions. Indeed, a compact soil structure increases the contact surface between aggregates and decreases the proportion of water that contributes to water transfer by creating unconnected pores (Richard et al., 2001). A greater part of the gas and water transfers occurs slowly through the textural porosity of the aggregates, instead of between aggregates. While the O_2 replenishment is low, favoring N_2O production, the N_2O transfer to the soil surface is also low, and thus, the probability of its reduction to N_2 is high. Typically, WFPS >90% can lead to N_2O reduction to N_2 (Ruser et al., 2006), because the N_2O-reductase is sensitive to inhibition by O_2 (Knowles, 1982). For example, by injecting ^{15}N-labeled N_2O at the bottom of a 22-cm long soil core, Klefoth et al. (2014) showed a complete consumption of the added N_2O at a WFPS of 90%.

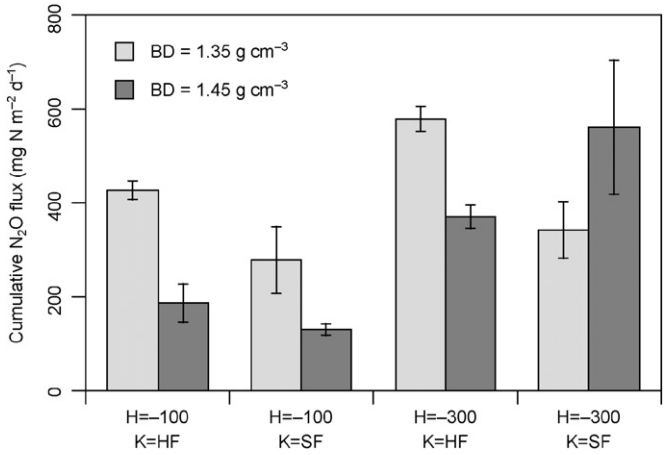

Fig. 5. Cumulative nitrous oxide fluxes at the end of the second wetting-drying cycle for samples of bulk density BD = 1.35 and 1.45 g cm^{-3} (H: pressure head applied, in hPa, K: saturated hydraulic conductivity of the porous plate, HF: high flow, SF: standard flow). Error bars represent standard error of the mean (n = 3).

In our study, cumulative N_2O fluxes were generally higher for BD = 1.35 than for BD = 1.45 g cm^{-3} samples, despite high denitrification rates for BD = 1.45 g cm^{-3} samples, as shown by the lower soil nitrate content at the end of the experiment (Table 3). To explain this trend, production/consumption processes have to be taken into account. Indeed, conditions were favorable for N_2O production by denitrification, because WFPS was >60% (Grundmann and Rolston, 1987; Hénault and Germon, 2000) during the wetting phase and most of the time during the drying phase. Moreover, WFPS was higher for every hydric phase for BD = 1.45 than for BD = 1.35 g cm^{-3} samples (Table 3), because BD = 1.45 g cm^{-3} samples had smaller pore diameters (Fig. 1). The high WFPS during wetting and in some drying treatments led to N_2O being reduced to N_2 (Letey et al., 1980; Weier et al., 1993), even during the drying phase. This could explain the low cumulative N_2O fluxes for BD = 1.45 compared to BD = 1.35 g cm^{-3} samples. When comparing repacked soil samples compacted then with different intensities, Harrison-Kirk et al. (2015) found similar findings: soil samples with the highest BD showed the lowest cumulative N_2O emissions and the highest cumulative N_2 emissions. They implicated the increased proportion of micropores in the compacted samples, leading to a longer time for these samples to drain, and thus providing favorable conditions for complete denitrification. In a range of WFPS comparable to our study (60, 75, and 100%), Klefoth et al. (2014) also demonstrated that the N_2O consumption depended on the interaction between BD and WFPS: N_2O consumption was higher for high WFPS values and high BD.

An additional explanation for the low cumulative N_2O fluxes of some BD = 1.45 g cm^{-3} samples is linked to the value of the air-entry potential and the imposed H. Indeed, the H values applied during our experiments were higher than the air-entry potential of the soil, providing favorable conditions for N_2O transport by gas diffusion, except for the BD = 1.45 g cm^{-3} and H = −100 hPa treatment. In these specific samples, very low outflows were measured compared with the other treatments. The air-entry potential value had a threshold effect on the N_2O fluxes, because as long as it was not reached, very few gas pathways were available for N_2O transport in the gas phase, leading to entrapment and lower N_2O fluxes at the soil surface. The threshold effect of the air-entry potential explains the dominating effect of H for the BD = 1.45 g cm^{-3} samples contrary to the BD = 1.35 g cm^{-3} samples, and the behavior of the H = −100 hPa, K = SF treatment of the BD = 1.45 g cm^{-3} samples, whose maximum N_2O flux during drying was

Table 4
Results of the ANOVA performed on the cumulative nitrous oxide emissions and bulk density (BD), pressure head applied (H), and saturated hydraulic conductivity of the porous plate (K).

	Df	Sum Sq	Mean Sq	F value	Pr(>F)	Eta Sq
BD	1	0.8828	0.8828	8.747	0.00926 **	0.12
H	1	2.7067	2.7067	26.820	<0.0001 ***	0.37
K	1	0.4002	0.4002	3.965	0.06381	0.05
BD×H	1	0.9290	0.9290	9.205	0.00790 **	0.13
BD×K	1	0.4603	0.4603	4.560	0.04852 *	0.06
H×K	1	0.1525	0.1525	1.511	0.23681	0.02
BD×H×K	1	0.1980	0.1980	1.962	0.18037	0.03
Residuals	16	1.6148	0.1009			0.22

lower than during wetting. On repacked soil samples, Balaine et al. (2013) showed that maximum N_2O fluxes occurred when the air-entry potential of the soil was reached. Thus, the role of BD was related to both production/consumption and transport processes, and BD had an effect during both the wetting and drying phases.

Contrasting results were found in the literature, since several observations also showed that dense soils can cause higher N_2O fluxes than loose soils (Balaine et al., 2013; Beare et al., 2009; Hansen et al., 1993; Ruser et al., 2006; Yamulki and Jarvis, 2002). For example, on intact soil cores, Beare et al. (2009) observed higher N_2O fluxes for dense soils (BD = 1.49 g cm^{-3} compared to BD = 1.01 g cm^{-3}), during both the wetting and drying phases. These high fluxes for high BD were often explained by a reduction of the air-filled porosity, leading to longer periods of high WFPS, favorable for N_2O production. The high N_2O fluxes of compacted soils have also been explained by the decrease of the mean pore diameter with compaction, which could increase the physical protection of organic matter and reduce the carbon availability for microorganisms (Breland and Hansen, 1996). Actually, denitrification seems to be enhanced for high BD, and the inconsistencies between the observations reported in the literature on the effect of BD on the N_2O emissions are related to the intensity of N_2 production.

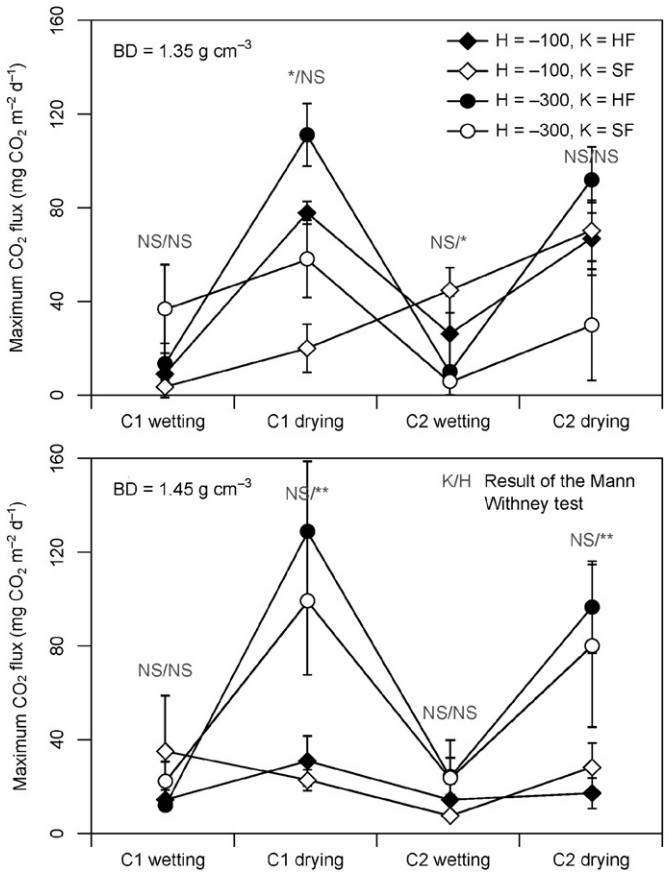

Fig. 6. Maximum carbon dioxide fluxes recorded during the four successive hydric steps (C1: first wetting-drying cycle, C2: second wetting-drying cycle) for soil samples of bulk density BD = 1.35 and 1.45 g cm^{-3} (H: pressure head applied, in hPa, K: saturated hydraulic conductivity of the porous plate, HF: high flow, SF: standard flow). Error bars represent standard error of the mean ($n = 3$).

4.3. Nitrous oxide production during wetting-drying cycles

Wetting-drying cycles are known to influence N_2O production. In our study, cumulative N_2O fluxes were always higher for C1 than for C2 during the wetting phase, and mainly higher for C1 than for C2 during the drying phase. Indeed, brief peaks were observed at the very beginning of the C1 wetting phase (Fig. 2). They were not shown at the beginning of the C2 wetting phase. Rewetting peaks have already been observed on undisturbed soil cores (e.g., Beare et al., 2009; Ciarlo et al., 2007; Rabot et al., 2014). Muhr et al. (2008) and Borken and Matzner (2009) listed several explanations for the increase in nitrogen mineralization after wetting a dry soil: it could be the result of an increase of the substrate availability caused by the dying of microorganisms during wetting, the release of intracellular substances by microorganisms as an adaptation to the water stress, or the disruption of physically protected organic matter during wetting. The intensity of the peak is especially high as the difference between the initial WFPS and the final WFPS is high (Guo et al., 2014). In the current study, the peak occurred just after the beginning of the wetting phase and was very short. Thus, this peak was rather linked to the release of carbon substrate during the preparation of the repacked soil samples (Del Grosso et al., 2000; Powlson, 1980; van Veen and Kuikman, 1990). Moreover, the easily available carbon substrates may have mainly been consumed during C1, providing less carbon for the C2 cycle (Fierer and Schimel, 2002). The high N_2O production during C1 led to N_2O accumulation into the soil, and higher N_2O fluxes during the C1 drying phase than during the C2 drying phase.

Soil drying over several days could be seen as a water stress for microorganisms. Muhr et al. (2008) observed a decrease in N_2O emissions after drying forest soil samples by evaporation during a period of 42 days. They hypothesized that the length of the drought period could influence total N_2O emissions by disrupting the microbial activity. By successively drying soils from saturation, to field capacity (approximately 75% WFPS), 60% WFPS, and 20% WFPS, Groffman and Tiedje (1988) showed a marked decrease in the N_2O fluxes produced by denitrification from saturation to field capacity in three soils of different textures. In the study of Groffman and Tiedje (1988), the desaturation took three days, as in the present experiment, but N_2O fluxes were recorded when samples were at their hydraulic equilibrium. So, no comparison can be done with the brief peaks observed at the beginning of the drying phase in this current study. In the present experiment, cumulative N_2O fluxes were higher for the H = −300 hPa than for the H = −100 hPa level for each treatment. The drying period probably did not affect the microbial activity and thus the cumulative N_2O fluxes, because of its short duration and the high remaining WFPS value.

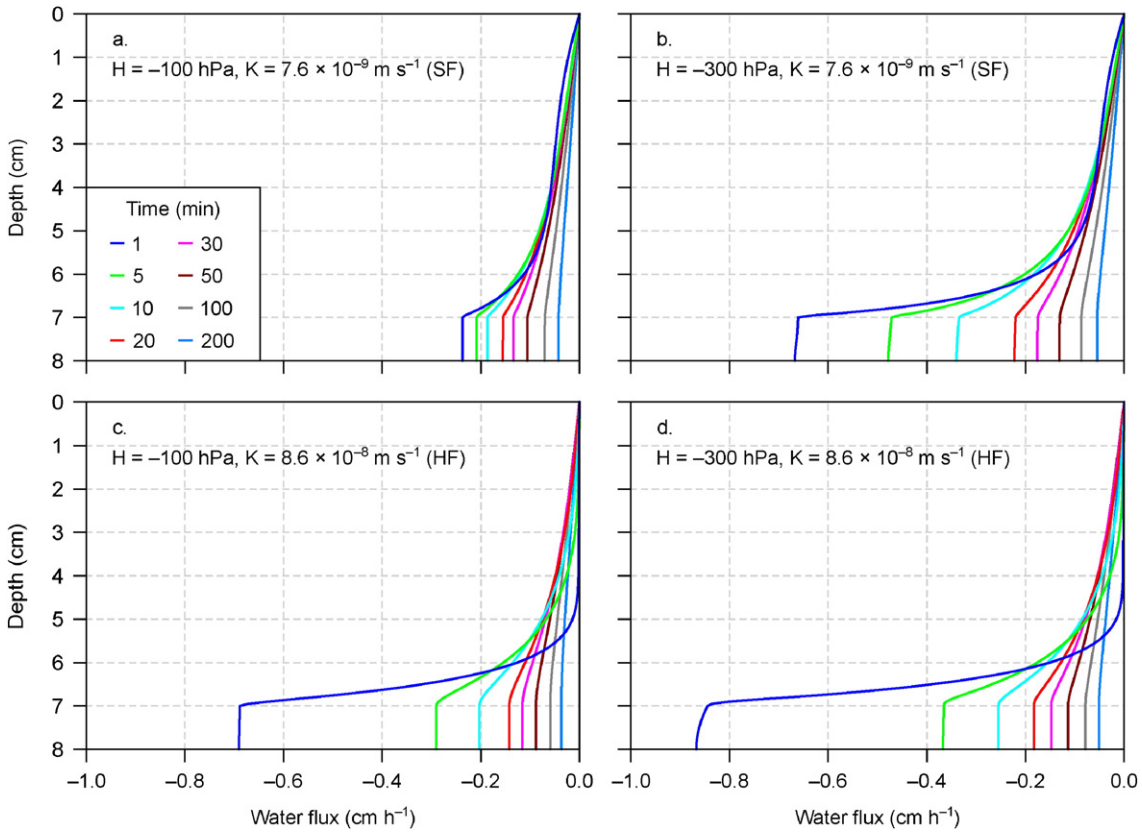

Fig. 7. Simulated profiles of water flux with time just after the beginning of the soil drying of a sample of bulk density BD = 1.35 g cm^{-3} (H: pressure head applied, K: saturated hydraulic conductivity of the porous plate). Because a drying phase is simulated, the water flux is negative.

4.4. Hierarchy of the controlling factors

Taking into account the whole data set, we ranked the importance of the three parameters tested: the higher impact on the cumulative N_2O emissions was observed for H, then BD, and finally K. The threshold effect of the air-entry potential caused a non-linearity of the response, which was explained for 13% by the interaction between BD and H in the ANOVA procedure. It is worth noting that the choice of the values we applied in this experiment had an important effect on the water flow, the N_2O emissions, and therefore on this ranking. The ANOVA on H, BD, and K accounted for 78% of the total variation of the N_2O emissions, so a further fraction remained unexplained. This unexplained fraction may be related to the heterogeneity of the soil samples in terms of carbon substrates, supposed to be the place of some hotspots of denitrification (Groffman et al., 2009; Parkin, 1987). This heterogeneity in carbon distribution between samples could be inferred from the high variability observed in the CO_2 fluxes (Fig. 6). Heterogeneity may also be referred to slight differences in the soil structure, despite the samples were repacked.

5. Conclusion

This study examined the effect of the soil water dynamics on N_2O emissions in repacked soil cores subjected to wetting-drying cycles. High temporal resolution of the N_2O measurements allowed capture of a brief peak at the beginning of the soil drying. Its intensity was large enough to affect cumulative N_2O fluxes at the time scale of the experiment. A similar peak dynamics was observed for CO_2, despite different optimal moisture conditions for its formation, implying that a physical process was responsible for the peak. Indeed, N_2O and CO_2 have been entrapped in the soil pore space and in the water phase during the wetting phase and have been released later during the soil drying. An exponential relationship between the maximum N_2O flux during drying and the outflow provided evidence of the importance of water flow processes, such as speed and degree of soil drying. Indeed, during drying, high N_2O fluxes were measured when the air-entry potential was reached, that is to say, when gas pathways were available for fast N_2O transport in the gas phase. Then, maximum and cumulative N_2O fluxes were highest for low BD and fast water flow during drainage. Samples with the highest BD had smaller pore sizes, leading to low outflows at a given negative pressure head, and giving more time for further reduction of N_2O to N_2.

Acknowledgments

We are grateful to D. Colosse, P. Courtemanche, and G. Giot for their technical help in the experimental design of this study. We also thank G. Giot and L. Gouny for hydraulic parameter measurements, and A. Ayzac and L. Cottenot for occasional assistance with N_2O measurements. Carbon and nitrogen analyses were graciously performed by the SAS Laboratoire. This work was supported by a Conseil Général du Loiret grant, by the Spatioflux program funded by the Région Centre, FEDER, INRA and BRGM, and by the Labex VOLTAIRE (ANR-10-LABX-100-01).

References

Balaine, N., Clough, T.J., Beare, M.H., Thomas, S.M., Meenken, E.D., Ross, J.G., 2013. Changes in relative gas diffusivity explain soil nitrous oxide flux dynamics. Soil Sci. Soc. Am. J. 77 (5), 1496–1505.

Bateman, E.J., Baggs, E.M., 2005. Contributions of nitrification and denitrification to N_2O emissions from soils at different water-filled pore space. Biol. Fertil. Soils 41 (6), 379–388.

Beare, M.H., Gregorich, E.G., St-Georges, P., 2009. Compaction effects on CO_2 and N_2O production during drying and rewetting of soil. Soil Biol. Biochem. 41 (3), 611–621.

Borken, W., Matzner, E., 2009. Reappraisal of drying and wetting effects on C and N mineralization and fluxes in soils. Glob. Chang. Biol. 15 (4), 808–824.
Breland, T.A., Hansen, S., 1996. Nitrogen mineralization and microbial biomass as affected by soil compaction. Soil Biol. Biochem. 28 (4–5), 655–663.
Buckingham, E., 1904. Contributions to our Knowledge to the Aeration of Soils. US Government Printing Office, Washington, DC.
Campbell, G.S., 1974. A simple method for determining unsaturated conductivity from moisture retention data. Soil Sci. 117 (6), 311–314.
Castellano, M.J., Schmidt, J.P., Kaye, J.P., Walker, C., Graham, C.B., Lin, H., Dell, C.J., 2010. Hydrological and biogeochemical controls on the timing and magnitude of nitrous oxide flux across an agricultural landscape. Glob. Chang. Biol. 16 (10), 2711–2720.
Ciais, P., Sabine, C., Bala, G., Bopp, L., Brovkin, V., Canadell, J., Chhabra, A., DeFries, R., Galloway, J., Heimann, M., Jones, C., Le Quéré, C., Myneni, R.B., Piao, S., Thornton, P., 2013. Carbon and other biogeochemical cycles. In: Stocker, T.F., et al. (Eds.), Climate Change 2013: The Physical Science Basis. Contribution of Working Group I to the Fifth Assessment Report of the Intergovernmental Panel on Climate Change. Cambridge University Press, Cambridge, UK and New York, NY, USA, pp. 465–570.
Ciarlo, E., Conti, M., Bartoloni, N., Rubio, G., 2007. The effect of moisture on nitrous oxide emissions from soil and the $N_2O/(N_2O + N_2)$ ratio under laboratory conditions. Biol. Fertil. Soils 43 (6), 675–681.
Clough, T.J., Jarvis, S.C., Dixon, E.R., Stevens, R.J., Laughlin, R.J., Hatch, D.J., 1998. Carbon induced subsoil denitrification of ^{15}N-labelled nitrate in 1 m deep soil columns. Soil Biol. Biochem. 31 (1), 31–41.
Clough, T.J., Sherlock, R.R., Rolston, D.E., 2005. A review of the movement and fate of N_2O in the subsoil. Nutr. Cycl. Agroecosyst. 72 (1), 3–11.
Del Grosso, S.J., Parton, W.J., Mosier, A.R., Ojima, D.S., Kulmala, A.E., Phongpan, S., 2000. General model for N_2O and N_2 gas emissions from soils due to denitrification. Glob. Biogeochem. Cycles 14 (4), 1045–1060.
Ekstrom, C., 2014. MESS. R package version 0.2–1. http://CRAN.R-project.org/package=MESS.
Fierer, N., Schimel, J.P., 2002. Effects of drying-rewetting frequency on soil carbon and nitrogen transformations. Soil Biol. Biochem. 34 (6), 777–787.
Groffman, P.M., Tiedje, J.M., 1988. Denitrification hysteresis during wetting and drying cycles in soil. Soil Sci. Soc. Am. J. 52 (6), 1626–1629.
Groffman, P.M., Butterbach-Bahl, K., Fulweiler, R.W., Gold, A.J., Morse, J.L., Stander, E.K., Tague, C., Tonitto, C., Vidon, P., 2009. Challenges to incorporating spatially and temporally explicit phenomena (hotspots and hot moments) in denitrification models. Biogeochemistry 93 (1–2), 49–77.
Grundmann, G.L., Rolston, D.E., 1987. A water function approximation to degree of anaerobiosis associated with denitrification. Soil Sci. 144 (6), 437–441.
Gu, J.X., Nicoullaud, B., Rochette, P., Pennock, D.J., Hénault, C., Cellier, P., Richard, G., 2011. Effect of topography on nitrous oxide emissions from winter wheat fields in Central France. Environ. Pollut. 159 (11), 3149–3155.
Guo, X.B., Drury, C.F., Yang, X.M., Reynolds, W.D., Fan, R.Q., 2014. The extent of soil drying and rewetting affects nitrous oxide emissions, denitrification, and nitrogen mineralization. Soil Sci. Soc. Am. J. 78 (1), 194–204.
Hansen, S., Mæhlum, J.E., Bakken, L.R., 1993. N_2O and CH_4 fluxes in soil influenced by fertilization and tractor traffic. Soil Biol. Biochem. 25 (5), 621–630.
Harrison-Kirk, T., Beare, M.H., Meenken, E.D., Condron, L.M., 2013. Soil organic matter and texture affect responses to dry/wet cycles: effects on carbon dioxide and nitrous oxide emissions. Soil Biol. Biochem. 57, 43–55.
Harrison-Kirk, T., Thomas, S.M., Clough, T.J., Beare, M.H., van der Weerden, T.J., Meenken, E.D., 2015. Compaction influences N_2O and N_2 emissions from ^{15}N-labeled synthetic urine in wet soils during successive saturation/drainage cycles. Soil Biol. Biochem. 88, 178–188.
Heincke, M., Kaupenjohann, M., 1999. Effects of soil solution on the dynamics of N_2O emissions: a review. Nutr. Cycl. Agroecosyst. 55 (2), 133–157.
Hénault, C., Germon, J.C., 2000. NEMIS, a predictive model of denitrification on the field scale. Eur. J. Soil Sci. 51 (2), 257–270.
IUSS Working Group WRB, 2014. World reference base for soil resources 2014: International soil classification system for naming soils and creating legends for soil maps. World Soil Resour. Rep.FAO, Rome, p. 106
Khalil, M.A.K., Rasmussen, R.A., Shearer, M.J., 2002. Atmospheric nitrous oxide: patterns of global change during recent decades and centuries. Chemosphere 47 (8), 807–821.
Klefoth, R.R., Clough, T.J., Oenema, O., van Groenigen, J.-W., 2014. Soil bulk density and moisture content influence relative gas diffusivity and the reduction of nitrogen-15 nitrous oxide. Vadose Zone J. 13 (11).
Knowles, R., 1982. Denitrification. Microbiol. Rev. 46 (1), 43–70.
Kroeckel, L., Stolp, H., 1986. Influence of the water regime on denitrification and aerobic respiration in soil. Biol. Fertil. Soils 2 (1), 15–21.
Letey, J., Valoras, N., Hadas, A., Focht, D.D., 1980. Effect of air-filled porosity, nitrate concentration, and time on the ratio of N_2O/N_2 evolution during denitrification. J. Environ. Qual. 9 (2), 227–231.
Linn, D.M., Doran, J.W., 1984. Effect of water-filled pore space on carbon dioxide and nitrous oxide production in tilled and nontilled soils. Soil Sci. Soc. Am. J. 48 (6), 1267–1272.
Mathieu, O., Hénault, C., Lévêque, J., Baujard, E., Milloux, M.J., Andreux, F., 2006. Quantifying the contribution of nitrification and denitrification to the nitrous oxide flux using ^{15}N tracers. Environ. Pollut. 144 (3), 933–940.
McNicol, G., Silver, W.L., 2014. Separate effects of flooding and anaerobiosis on soil greenhouse gas emissions and redox sensitive biogeochemistry. J. Geophys. Res. Biogeosci. 119 (4), 557–566.
Mualem, Y., 1976. A new model for predicting the hydraulic conductivity of unsaturated porous media. Water Resour. Res. 12 (3), 513–522.
Muhr, J., Goldberg, S.D., Borken, W., Gebauer, G., 2008. Repeated drying-rewetting cycles and their effects on the emission of CO_2, N_2O, NO, and CH_4 in a forest soil. J. Plant Nutr. Soil Sci. 171 (5), 719–728.
Parkin, T.B., 1987. Soil microsites as a source of denitrification variability. Soil Sci. Soc. Am. J. 51 (5), 1194–1199.
Powlson, D.S., 1980. The effects of grinding on microbial and non-microbial organic matter in soil. J. Soil Sci. 31 (1), 77–85.
R Core Team, 2015. R: a language and environment for statistical computing. R Foundation for Statistical Computing, Vienna, Austria (URL: http://www.R-project.org/).
Rabot, E., Hénault, C., Cousin, I., 2014. Temporal variability of nitrous oxide emissions by soils as affected by hydric history. Soil Sci. Soc. Am. J. 78 (2), 434–444.
Rabot, E., Lacoste, M., Hénault, C., Cousin, I., 2015. Using X-ray computed tomography to describe the dynamics of nitrous oxide emissions during soil drying. Vadose Zone J. 14 (8).
Richard, G., Cousin, I., Sillon, J.F., Bruand, A., Guérif, J., 2001. Effect of compaction on the porosity of a silty soil: influence on unsaturated hydraulic properties. Eur. J. Soil Sci. 52 (1), 49–58.
Ruser, R., Flessa, H., Russow, R., Schmidt, G., Buegger, F., Munch, J.C., 2006. Emission of N_2O, N_2 and CO_2 from soil fertilized with nitrate: effect of compaction, soil moisture and rewetting. Soil Biol. Biochem. 38 (2), 263–274.
Ruy, S., Mohrath, D., Bertuzzi, P., Bruckler, L., 2004. ESPAS 1.0, INRA-CSE, Avignon, France.
Sexstone, A.J., Parkin, T.B., Tiedje, J.M., 1985. Temporal response of soil denitrification rates to rainfall and irrigation. Soil Sci. Soc. Am. J. 49 (1), 99–103.
Simunek, J., Sejna, M., van Genuchten, M.T., 2008. HYDRUS-1D, V. 4.16. Code for Simulating the one-Dimensional Movement of Water, Heat, and Multiple Solutes in variably Saturated Porous Media.
Tamari, S., Bruckler, L., Halbertsma, J., Chadoeuf, J., 1993. A simple method for determining soil hydraulic properties in the laboratory. Soil Sci. Soc. Am. J. 57 (3), 642–651.
van Genuchten, M.T., 1980. A closed-form equation for predicting the hydraulic conductivity of unsaturated soils. Soil Sci. Soc. Am. J. 44 (5), 892–898.
van Veen, J.A., Kuikman, P.J., 1990. Soil structural aspects of decomposition of organic matter by micro-organisms. Biogeochemistry 11 (3), 213–233.
Weier, K.L., Doran, J.W., Power, J.F., Walters, D.T., 1993. Denitrification and the dinitrogen/nitrous oxide ratio as affected by soil water, available carbon, and nitrate. Soil Sci. Soc. Am. J. 57 (1), 66–72.
Wind, G.P., 1968. Capillary conductivity data estimated by a simple method. In: Rijtema, P.E., et al. (Eds.), Water in the Unsaturated Zone. Proceedings of the Wageningen Symposium, Vol. 1, June 1966. IAHS, Unesco, Belgium, pp. 181–191.
Wollersheim, R., Trolldenier, G., Beringer, H., 1987. Effect of bulk density and soil water tension on denitrification in the rhizosphere of spring wheat (*Triticum vulgare*). Biol. Fertil. Soils 5 (3), 181–187.
Xing, H.T., Wang, E.L., Smith, C.J., Rolston, D., Yu, Q., 2011. Modelling nitrous oxide and carbon dioxide emission from soil in an incubation experiment. Geoderma 167-168, 328–339.
Yamulki, S., Jarvis, S.C., 2002. Short-term effects of tillage and compaction on nitrous oxide, nitric oxide, nitrogen dioxide, methane and carbon dioxide fluxes from grassland. Biol. Fertil. Soils 36 (3), 224–231.